




## Article

# Preparation and Evaluation of 6-Gingerol Derivatives as Novel Antioxidants and Antiplatelet Agents

Sara H. H. Ahmed <sup>1,†,‡</sup>, Tímea Gonda <sup>1,†</sup>, Orinamhe G. Agbadua <sup>1</sup>, Gábor Girst <sup>1</sup>, Róbert Berkecz <sup>2</sup>, Norbert Kúsz <sup>1</sup>, Meng-Chun Tsai <sup>3</sup>, Chin-Chung Wu <sup>3</sup>, György T. Balogh <sup>4,5</sup> and Attila Hunyadi <sup>1,6,\*</sup>

<sup>1</sup> Institute of Pharmacognosy, University of Szeged, H-6720 Szeged, Hungary

<sup>2</sup> Institute of Pharmaceutical Analysis, University of Szeged, H-6720 Szeged, Hungary

<sup>3</sup> Graduate Institute of Natural Products, Kaohsiung Medical University, Kaohsiung 807, Taiwan

<sup>4</sup> Institute of Pharmacodynamics and Biopharmacy, University of Szeged, H-6720 Szeged, Hungary

<sup>5</sup> Department of Chemical and Environmental Process Engineering,

Budapest University of Technology and Economics, H-1111 Budapest, Hungary

<sup>6</sup> Interdisciplinary Centre of Natural Products, University of Szeged, H-6720 Szeged, Hungary

\* Correspondence: hunyadi.attila@szte.hu; Tel.: +36-62545557

† These authors contributed equally to this work.

‡ On leave from the Department of Pharmaceutical Chemistry, Faculty of Pharmacy, University of Khartoum, 11111 Khartoum, Sudan.

**Abstract:** Ginger (*Zingiber officinale*) is widely used as a spice and a traditional medicine. Many bioactivities have been reported for its extracts and the isolated compounds, including cardiovascular protective effects. Different pathways were suggested to contribute to these effects, like the inhibition of platelet aggregation. In this study, we synthesised fourteen 6-gingerol derivatives, including eight new compounds, and studied their antiplatelet, COX-1 inhibitor, and antioxidant activities. In silico docking of selected compounds to *h*-COX-1 enzyme revealed favourable interactions. The investigated 6-gingerol derivatives were also characterised by in silico and experimental physico-chemical and blood–brain barrier-related parameters for lead and preclinical candidate selection. 6-Shogaol (**2**) was identified as the best overall antiplatelet lead, along with compounds **3** and **11** and the new compound **17**, which require formulation to optimize their water solubility. Compound **5** was identified as the most potent antioxidant that is also promising for use in the central nervous system (CNS).

**Keywords:** ginger; 6-gingerol; cardiovascular disease; antiplatelet; cyclooxygenase-1; antioxidant; pharmacokinetics; BBB-PAMPA



**Citation:** Ahmed, S.H.H.; Gonda, T.; Agbadua, O.G.; Girst, G.; Berkecz, R.; Kúsz, N.; Tsai, M.-C.; Wu, C.-C.; Balogh, G.T.; Hunyadi, A.

Preparation and Evaluation of 6-Gingerol Derivatives as Novel Antioxidants and Antiplatelet Agents. *Antioxidants* **2023**, *12*, 744. <https://doi.org/10.3390/antiox12030744>

Academic Editor: María Jesús Rodríguez-Yoldi

Received: 16 February 2023

Revised: 10 March 2023

Accepted: 13 March 2023

Published: 17 March 2023



**Copyright:** © 2023 by the authors. Licensee MDPI, Basel, Switzerland. This article is an open access article distributed under the terms and conditions of the Creative Commons Attribution (CC BY) license (<https://creativecommons.org/licenses/by/4.0/>).

## 1. Introduction

Ginger, *Zingiber officinale* Rosc. (Zingiberaceae), is a well-known culinary plant and herbal remedy for many diseases. Ginger root extracts have been reported efficient against nausea and vomiting, diarrhoea, inflammatory conditions, metabolic syndrome, hepatotoxicity, and cardiovascular diseases [1–3]. The plant is rich in bioactive secondary metabolites including terpenes and phenolic compounds. The latter group consists mainly of gingerols, shogaols, paradols, and zingerone [4,5], among which 6-gingerol has been reported to be the most abundant in fresh ginger roots [6].

A plethora of preclinical studies demonstrated antioxidant [7,8], antimicrobial [9,10], anti-inflammatory [11], neuroprotective [12], antiplatelet [13], anti-obesity [14], antihepatotoxic [15], and anticancer effects for 6-gingerol [16]. Great efforts have been devoted to synthesizing and studying semisynthetic derivatives inspired by the structure of 6-gingerol. In our recent review, we have discussed such studies covering more than 150 semi-synthetic compounds, based on which the antiplatelet activity of gingerol derivatives seems to be the most promising [17].

Cardiovascular diseases (CVDs) represent a leading cause of death worldwide, with approximately 17.9 million deaths every year, according to the World Health Organisation (WHO) reports [18]. Many factors are implicated in CVDs' development and progression, including an imbalance between haemostasis and thrombosis [19]. Platelets represent a key element in this due to their crucial role in the coagulation cascade, and antiplatelet therapies are of fundamental importance in the treatment of cardiovascular and in cerebrovascular pathologies [20]. Cyclooxygenase 1 (COX-1), constitutively expressed in all tissues, is a key regulator of platelet activation [21]. It has also been reported that high reactive oxygen species (ROS) levels contribute to platelet activation and play a causal role in CVDs [22]. While currently marketed antiplatelet drugs are undoubtedly efficient, all of them have some clinical limitations [23,24]. Aspirin is a good example of this: it significantly reduces morbidity in CVDs [25], but its gastrointestinal (GI) side effects limit its use, especially in those patients who are susceptible to, or already experience, gastrointestinal ulcers [26]. Therefore, there is still a need for additional safe and efficient alternatives.

Phytotherapy may offer complementary supportive treatment options for CVDs [27], and ginger has been suggested for this purpose [3] due to its effectiveness in reducing platelet aggregation [2,28–31]. Related clinical studies have also been conducted. Young et al. reported an increase in the antiplatelet activity upon ginger consumption by nifedipine-treated patients [32]. A similar effect was observed upon ginger administration in patients with coronary artery disease [33]. On the other hand, no effect was observed on platelet aggregation and coagulation when ginger was administered to healthy humans [34,35]. Furthermore, promising results have also been reported for the antiplatelet activity of semi-synthetic gingerol derivatives [36,37].

Ginger and many of its constituents, particularly gingerols and shogaols, are considered potent antioxidants through scavenging various biologically relevant free radicals [38] and modulating a range of redox signalling pathways [17]. It is worth mentioning that the modulation of antioxidant pathways by 6-gingerol protects H9c2 cardiomyocytes from hypoxia-induced damage [39], and that ginger constituents also inhibit the NLRP3 inflammasome [40] that has a key importance concerning cardiovascular health [41,42].

In the present work, we aimed to introduce different changes to the skeleton of 6-gingerol, and test the antiplatelet, COX-1 inhibitory, and antioxidant activity to evaluate their pharmacodynamic potential as cardio- and cerebrovascular protective agents. Furthermore, it was also our aim to characterize key physicochemical parameters and central nervous system (CNS)-related basic pharmacokinetic behaviour of the gingerol derivatives, including their *in vitro* blood–brain barrier permeability, to evaluate their additional potential as CNS antioxidants.

## 2. Materials and Methods

### 2.1. General Information

Reagents were purchased from Sigma (Merck KGaA, Darmstadt, Germany) unless otherwise stated. Solvents (analytical grade for synthetic work and flash chromatography purifications and high-performance liquid chromatography (HPLC)-grade for analytical and preparative HPLC work) were obtained from Macron Fine Chemicals (Avantor Performance Materials, Center Valley, PA, USA), Chem-Lab NV (Zedelgem, Belgium), VWR International S.A.S., and Fontenay-sous-Bois, France. A commercial ginger extract was purchased from Xi'an Pincredit Bio-Tech Co., Ltd., China. COX-1 kit was obtained from VWR International Kft. Debrecen, Hungary (original source: Biovision Inc., Milpitas, CA, USA).

For purification of the compounds, flash chromatography was used on a CombiFlashfi Rf+ Lumen apparatus (TELEDYNE Isco, Lincoln, NE, USA) equipped with evaporative light scattering (ELS) and diode array detectors, and the stationary phases were RediSep prefilled silica columns and RediSep cartridges (Teledyne Isco Inc., Lincoln, NE, USA). Hereinafter, solvent system compositions are always given in volumetric ratios.

Preparative purifications over RP-HPLC were performed on a Kinetex XB C18 (5 µm, 250 × 21.2 mm) column on an Armen Spot Prep II integrated HPLC purification system

(Gilson, Middleton, WI, USA) with dual-wavelength detection, with an adequately chosen combination of acetonitrile–water, and a flow rate of 15 mL/min. The purity of the compounds obtained was determined by RP-HPLC analyses on a system of two Jasco PU 2080 pumps, a Jasco AS-2055 Plus intelligent sampler connected to a JASCO LC-Net II/ADC equipped with a Jasco MD-2010 Plus PDA detector (Jasco International Co. Ltd., Hachioji, Tokyo, Japan) utilizing a Kinetex C-18 (5  $\mu$ m, 250  $\times$  4.6 mm) column (Phenomenex Inc., Torrance, CA, USA) and applying a gradient of 30%–100% aqueous AcN in 30 min followed by 100% AcN for 10 min with a flow rate of 1 mL/min. Analysis of samples from the PAMPA and kinetic solubility assays was performed the same way, by using 3-point calibrations and integrating each compound at its UV absorption maximum.

$^1\text{H}$ - and  $^{13}\text{C}$  NMR spectra were recorded in  $\text{CDCl}_3$  or  $\text{CD}_3\text{OD}$  using 5 mm tubes at room temperature on a Bruker DRX-500 spectrometer at 500 ( $^1\text{H}$ ) and 125 ( $^{13}\text{C}$ ) MHz with the deuterated solvents' signal taken as reference. The heteronuclear single quantum coherence (HSQC), heteronuclear multiple bond correlation (HMBC),  $^1\text{H}$ - $^1\text{H}$  correlation spectroscopy (COSY), and nuclear Overhauser effect spectroscopy (NOESY) spectra were obtained using the standard Bruker pulse programs.  $^1\text{H}$ - and  $^{13}\text{C}$  NMR spectra for compounds **4**, **12**, **14**–**18** and **22** are available in the Supplementary Materials, Figures S9–S24. High resolution mass spectroscopy (HRMS) spectra were recorded on a Q-Exactive Plus hybrid quadrupole-orbitrap mass spectrometer (Thermo Scientific, Waltham, MA, USA) equipped with heated electrospray ionisation (HESI-II) probe that was used in positive or negative mode per needed. HRMS spectra for compounds **4**, **12**, **14**–**18** and **22** are available as Supplementary Materials, Figures S1–S8.

All bioactivity data processing, including the calculation of inhibition percentage, mean and corresponding standard error of the mean (SEM), and  $\text{IC}_{50}$  values, was performed by GraphPad Prism 8.0 (La Jolla, CA, USA).  $\text{IC}_{50}$  values were calculated from the sigmoidal dose–response curves obtained by the log(inhibitor) vs. response and variable slope (DPPH assay) or the log(inhibitor) vs. normalised response and variable slope nonlinear regression model. On the results obtained, no statistical evaluation was performed; instead, differences greater than two-fold were considered relevant. Plotting of the antiplatelet and COX-1 inhibitory  $\text{IC}_{50}$  values and the linear regression of the data was performed by Microsoft Excel.

## 2.2. Isolation and Semi-synthesis

### 2.2.1. Purification of 6-gingerol

#### ((S)-5-hydroxy-1-(4-hydroxy-3-methoxyphenyl)decan-3-one) (**1**)

Ginger extract was purchased from Xi'an Pincredit Bio-Tech Co., Ltd., Xi'an, China. 6-Gingerol (**1**) was purified from the crude extract at up to a 4 g scale using flash chromatography (Silica, gradient elution of 0–10% of acetone in *n*-hexane) and obtained as a dark yellow oil (36.8% yield). 6-Gingerol (**1**) was then utilised to synthesize 6-shogaol (**2**), and subsequently 4,5-dihydro-6-shogaol (**3**), as published previously [43]. Compound **11** was derived from vanillin (**7**) and 2,4-nonanedione (**10**), and compound **13** from compound **11**, as published previously [44].

### 2.2.2. Synthesis of 1-(4-hydroxy-3-methoxyphenyl)decan-3-one oxime (**4**)

Hydroxylamine hydrochloride (228 mg, 3.3 mmol) was added to a solution of compound **3** (304 mg, 1.1 mmol) in MeOH (5 mL) at room temperature. The reaction was monitored by thin-layer chromatography (TLC), the reaction mixture was purified by flash chromatography (Silica, gradient elution of 0–30% of EtOAc in *n*-hexane) to afford compound **4**, a pale-yellow solid (255 mg, 74.8%) [45].

Compound **4**. HRESIMS:  $\text{C}_{17}\text{H}_{27}\text{NO}_3$ ,  $[\text{M}+\text{H}]^+$   $m/z = 294.20694$  (calcd 294.20692),  $^1\text{H}$  NMR (500 MHz, in  $\text{CDCl}_3$ ):  $\delta_{\text{H}}$  6.83 (m, 1H), 6.70 (dd, 2H,  $J = 13.8, 7.6$  Hz), 3.88 (d, 3H,  $J = 3.5$  Hz), 3.48 (s, 1H), 2.77 (q, 2H,  $J = 8.0$  Hz), 2.60 (m, 1H), 2.46 (m, 1H), 2.36 (m, 1H), 2.10 (t, 1H,  $J = 7.6$  Hz), 1.50 (m, 2H), 1.31 (m, 2H), 1.28 (m, 7H), 0.88 (td, 3H,  $J = 7.0, 2.9$  Hz) ppm.  $^{13}\text{C}$  NMR (125 MHz, in  $\text{CDCl}_3$ ):  $\delta_{\text{C}}$  161.8, 161.7, 146.6, 144.1, 144.0, 133.6, 133.4, 121.0, 114.5, 111.1, 56.1, 36.4, 34.6, 32.5, 31.9, 31.5, 30.0, 30.0, 29.4, 29.2, 27.9, 26.4, 25.8, 22.8, 14.2.

### 2.2.3. Synthesis of (3*R*,5*S*)-1-(4-hydroxy-3-methoxyphenyl)decane-3,5-diol (**5**) and (3*S*,5*S*)-1-(4-hydroxy-3-methoxyphenyl)decane-3,5-diol (**6**)

Compound **1** (100 mg, 0.34 mmol) was dissolved in EtOH (10 mL) and NaBH<sub>4</sub> was added (38 mg, 1 mmol). The reaction was monitored by means of TLC and after completion (1 h) the solvent was evaporated in vacuo and water (20 mL) was added to the residue. The aqueous phase was extracted with EtOAc (3 × 20 mL), and the combined organic phase was dried over Na<sub>2</sub>SO<sub>4</sub>, filtered, and evaporated in vacuo resulting in a yellow oil (85 mg, 84%), which contained the gingerdiols in high purity (>95%), which were separated via preparative HPLC (50% aqueous AcN) to yield compound **5** as a faint yellow oil, and compound **6** as a white powder. The compounds' MS and NMR spectra were in good agreement with the literature data [46].

### 2.2.4. Synthesis of (*E*)-1-(4-hydroxyphenyl)dec-1-ene-3,5-dione (**12**)

*p*-Hydroxybenzaldehyde **8** (1000 mg, 8.2 mmol), boron trioxide (2280 mg, 32.8 mmol), and 2,4-nonanedione (2800 mg, 24.6 mmol) were mixed with 2 mL of DMF and heated to 90 °C. A solution of isobutylamine (150 mg = 202 μL, 4 mmol) in 2 mL of DMF was added dropwise over 2 h. The reaction mixture was stirred at 90 °C for 1 h then 50 mL of water was added. The resulting mixture was stirred at 60 °C for 1 h at room temperature overnight. The reaction mixture was extracted with EtOAc and the solvent was evaporated. Purification by flash chromatography (Silica, gradient elution, 5–10% EtOAc in *n*-hexane) afforded compound **12**, a yellow solid (179 mg, 8.5%) [44].

Compound **12**. HRESIMS: C<sub>16</sub>H<sub>20</sub>O<sub>3</sub>, [M–H]<sup>−</sup> *m/z* = 259.1332, (calcd 260.13342), <sup>1</sup>H NMR (500 MHz, in CD<sub>3</sub>OD): δ<sub>H</sub> 7.57 (d, 1H, *J* = 15.9 Hz), 7.50 (d, 2H, *J* = 8.6 Hz), 6.84 (m, 2H), 6.51 (d, 1H, *J* = 15.9 Hz), 2.42 (m, 2H), 1.67 (p, 2H, *J* = 7.7, 7.3 Hz), 1.39 (m, 4H), 0.97 (t, 3H, *J* = 7.0 Hz) ppm. <sup>13</sup>C NMR (125 MHz, in CD<sub>3</sub>OD): δ<sub>C</sub> 201.6, 179.6, 160.9, 141.3, 2 × 131.0, 128.1, 120.6, 2 × 116.9, 44.3, 40.9, 32.6, 26.5, 23.5, 14.3.

### 2.2.5. Synthesis of 2-methoxy-4-(2-(3-pentyl-1H-pyrazol-5-yl)ethyl)phenol (**14**), 4-(2-(3-pentyl-1H-pyrazol-5-yl)ethyl)phenol (**15**), and (*E*)-4-(2-(3-pentyl-1H-pyrazol-5-yl)vinyl)phenol (**16**)

To a stirred solution of compounds **11** or **12** (164 mg, 0.57 mmol/100 mg, 0.38 mmol) in ethanol (2 mL), hydrazine monohydrate (71 mg = 71 μL, 1.4 mmol/134 mg = 48 μL, 2.67 mmol) and a catalytic amount of concentrated HCl were added. The reaction mixture was refluxed for 6 h, cooled to ambient temperature, evaporated in vacuo, and purified using preparative HPLC (MeCN: H<sub>2</sub>O 40:60 for compound **14** and 42:58 for **15** and **16**) to afford compounds **14** (270 mg, 17.8%), **15**, (22 mg, 22.3%) or **16**, (23 mg, 23.6%) as pale-yellow solids [47].

Compound **14**. HRESIMS: C<sub>17</sub>H<sub>24</sub>N<sub>2</sub>O<sub>2</sub>, [M+H]<sup>+</sup> *m/z* = 289.19111 (calcd 289.19160). <sup>1</sup>H NMR (CDCl<sub>3</sub>, 500 MHz): δ<sub>H</sub> 6.83 (d, 1H, *J* = 8.0 Hz), 6.70 (dd, 1H, *J* = 8.0, 2.0 Hz), 6.67 (d, 1H, *J* = 2.0 Hz), 5.84 (s, 1H), 3.84 (s, 3H), 3.48 (s, 1H), 2.89 (m, 4H), 2.59 (t, 2H, *J* = 7.7 Hz), 1.64 (m, 2H), 1.35 (m, 2H), 1.33 (m, 2H), 0.90 (t, 3H, *J* = 7.1 Hz) ppm. <sup>13</sup>C NMR (125 MHz, in CDCl<sub>3</sub>): δ<sub>C</sub> 146.6, 144.2, 133.6, 121.2, 114.5, 111.3, 102.6, 56.1, 35.6, 31.7, 29.6, 29.2, 27.0, 22.6, 14.1.

Compound **15**. HRESIMS: C<sub>16</sub>H<sub>22</sub>N<sub>2</sub>O, [M+H]<sup>+</sup> *m/z* = 259.18057 (calcd 259.18104), <sup>1</sup>H NMR (500 MHz, in CDCl<sub>3</sub>): δ<sub>H</sub> 6.99 (d, 2H, *J* = 8.4 Hz), 6.71 (d, 2H, *J* = 8.5 Hz), 5.86 (s, 1H), 3.48 (s, 1H), 2.88 (t, 2H, *J* = 3.9 Hz), 2.87 (t, 2H, *J* = 4.2 Hz), 2.59 (t, 2H, *J* = 7.7 Hz), 1.63 (m, 2H), 1.34 (m, 2H), 1.31 (t, 2H, *J* = 3.9 Hz), 0.90 (t, 3H, *J* = 7.1 Hz) ppm. <sup>13</sup>C NMR (125 MHz, in CDCl<sub>3</sub>): δ<sub>C</sub> 154.7, 149.4, 148.9, 133.1, 2 × 129.6, 2 × 115.6, 102.6, 34.9, 31.6, 29.3, 29.1, 27.1, 22.6, 14.1.

Compound **16**. HRESIMS: C<sub>16</sub>H<sub>20</sub>N<sub>2</sub>O, [M+H]<sup>+</sup> *m/z* = 257.16489 (calcd 257.16539), <sup>1</sup>H NMR (500 MHz, in CD<sub>3</sub>OD): δ<sub>H</sub> 7.34 (d, 2H, *J* = 8.6 Hz), 7.01 (d, 1H, *J* = 16.5 Hz), 6.85 (d, 1H, *J* = 16.5 Hz), 6.77 (d, 2H, *J* = 8.6 Hz), 6.24 (s, 1H), 2.62 (t, 2H, *J* = 7.6 Hz), 1.67 (m, 2H), 1.38 (m, 2H), 1.36 (m, 2H), 0.92 (t, 3H, *J* = 6.8 Hz) ppm. <sup>13</sup>C NMR (125 MHz, in CD<sub>3</sub>OD): δ<sub>C</sub> 158.6, 131.1, 130.2, 2 × 128.8, 2 × 116.6, 103.8, 32.6, 30.3, 23.4, 14.3.

### 2.2.6. Synthesis of (*E*)-2-methoxy-4-(2-(3-pentylisoxazol-5-yl)vinyl)phenol (**17**) and (*E*)-4-(2-(3-pentylisoxazol-5-yl)vinyl)phenol (**18**)

Hydroxylamine hydrochloride (144 mg, 2.1 mmol/134 mg, 1.9 mmol) and pyridine (165 mg = 169  $\mu$ L, 2.1 mmol/152 mg = 155  $\mu$ L, 1.9 mmol) were added to a stirred solution of compounds **11** and **12** separately (122 mg, 0.42 mmol/100 mg, 0.38 mmol) in ethanol (4 mL) and refluxed for 6 hrs. The reaction was monitored by TLC. Subsequently, the mixture was cooled to ambient temperature, evaporated in vacuo, and purified by flash chromatography (Silica, gradient elution, 0–20% acetone in *n*-hexane) to afford compound **17**, a pale-yellow solid (96 mg, 79.3%), while product **18** was obtained as a pure compound from the reaction mixture as a pale-yellow solid (98 mg, 99%) [47].

Compound **17**. HRESIMS:  $C_{17}H_{21}NO_3$ ,  $[M+H]^+$   $m/z$  = 288.15999 (calcd 288.15996),  $^1H$  NMR (500 MHz, in  $CDCl_3$ ):  $\delta_H$  7.22 (d, 1H,  $J$  = 16.4 Hz), 7.04 (dd, 1H,  $J$  = 8.1, 2.0 Hz), 7.01 (d, 1H,  $J$  = 2.0 Hz), 6.92 (d, 1H,  $J$  = 8.1 Hz), 6.77 (d, 1H,  $J$  = 16.4 Hz), 6.06 (s, 1H), 5.77 (s, 1H), 3.95 (s, 3H), 2.66 (t, 2H,  $J$  = 7.5 Hz), 1.68 (m, 2H), 1.37 (m, 2H), 1.36 (m, 2H), 0.91 (t, 3H,  $J$  = 7.2 Hz) ppm.  $^{13}C$  NMR (125 MHz, in  $CDCl_3$ ):  $\delta_C$  168.5, 164.6, 147.0, 134.6, 128.5, 121.5, 114.9, 111.3, 108.9, 100.6, 56.1, 31.5, 28.2, 26.2, 22.5, 14.1.

Compound **18**. HRESIMS:  $C_{16}H_{19}NO_2$ ,  $[M-H]^-$   $m/z$  = 256.13644 (calcd 256.13375).  $^1H$  NMR (500 MHz, in  $CDCl_3$ ):  $\delta_H$  7.39 (dd, 2H,  $J$  = 8.6, 1.8 Hz), 7.23 (d, 1H,  $J$  = 16.4 Hz), 6.85 (dt, 2H,  $J$  = 8.6, 2.9, 2.1 Hz), 6.77 (d, 1H,  $J$  = 16.4 Hz), 6.06 (s, 1H), 3.49 (s, 1H), 2.66 (t, 2H,  $J$  = 7.5 Hz), 1.68 (m, 2H), 1.36 (m, 2H), 1.35 (m, 2H), 0.90 (t, 3H,  $J$  = 7.2 Hz) ppm.  $^{13}C$  NMR (125 MHz, in  $CDCl_3$ ):  $\delta_C$  168.7, 164.6, 157.1, 134.4, 2  $\times$  128.8, 128.6, 2  $\times$  116.0, 111.2, 100.6, 31.5, 28.2, 26.2, 22.5, 14.0.

### 2.2.7. Synthesis of *N*-heptyl-3-(4-hydroxyphenyl) propenamide (**22**)

A solution of compound **21** (300 mg, 1.5 mmol) in dry  $CH_2Cl_2$  (10 mL) was cooled to 0  $^\circ C$ , DCC (316 mg) and DMAP (18 mg, 0.2 mmol) were added, and the mixture was stirred for 1 h at 0  $^\circ C$ , then heptylamine (153 mg = 0.197 mL) was added and the reaction was monitored over TLC. Subsequently, the solvent was evaporated, redissolved in dichloromethane, washed with  $NaHCO_3$  solution, and the organic phase was evaporated to dryness. The product was purified by flash chromatography (Silica, gradient elution of 20–30% acetone in *n*-hexane) to yield compound **22** as a white solid (431 mg, 92.7%) [48].

Compound **22**. HRESIMS:  $C_{17}H_{27}NO_3$ ,  $[M+H]^+$   $m/z$  = 294.20680, (calcd 294.20692),  $^1H$  NMR (500 MHz, in  $CDCl_3$ ):  $\delta_H$  6.83 (d, 1H,  $J$  = 8.1 Hz), 6.72 (d, 1H,  $J$  = 2.0 Hz), 6.68 (dd, 1H,  $J$  = 8.0, 2.0 Hz), 5.47 (s, 1H), 3.87 (s, 3H), 3.20 (td, 2H,  $J$  = 7.2, 5.7 Hz), 2.89 (t, 2H,  $J$  = 7.5 Hz), 2.42 (t, 2H,  $J$  = 7.5 Hz), 1.43 (m, 2H), 1.26 (m, 8H), 0.88 (t, 3H,  $J$  = 6.9 Hz) ppm.  $^{13}C$  NMR (125 MHz, in  $CDCl_3$ ):  $\delta_C$  172.2, 146.6, 144.2, 133.0, 121.0, 114.5, 111.2, 56.3, 39.7, 39.2, 31.9, 31.7, 29.8, 29.1, 27.0, 22.7, 14.2.

## 2.3. Biological Activity

### 2.3.1. Antiplatelet Activity

Human platelet suspension ( $3 \times 10^8$  /mL in Tyrode's buffer) was prepared as previously described [49]. The protocol for this study was approved by the institutional review board of Kaohsiung Medical University Hospital (Kaohsiung City, Taiwan). Platelets pre-treated with DMSO (vehicle control) or test compounds were stimulated with arachidonic acid (AA), and platelet aggregation was measured using turbidimetric aggregometer (Chrono-Log Co., Havertown, PA, USA) at 37  $^\circ C$  under stirring conditions (1200 rpm).

### 2.3.2. 1,1-Diphenyl-2-picrylhydrazyl (DPPH) Scavenging Activity

DPPH (1,1-diphenyl-2-picrylhydrazyl) was purchased from Thermo Fisher Scientific. DPPH free radical scavenging assay was performed with some modifications based on the method by Fukomoto et al. [50]. Briefly, in a 96-well microplate, microdilutions of samples (100  $\mu$ L, starting from 200  $\mu$ M in HPLC grade MeOH) were made and 100  $\mu$ L of DPPH reagent (100  $\mu$ M in MeOH) was added. After 30 min at room temperature in the dark, the absorbance was measured at 550 nm using a FluoStar Optima plate reader (software

version 2.20R2, BMG Labtech Ortenberg, Germany). For the blank control, MeOH was used. The scavenging activity was calculated as Inhibition (%) =  $(A_0 - A_s)/A_0 \times 100$ , and IC<sub>50</sub> values were calculated by GraphPad Prism 8.0 (La Jolla, CA, USA).

### 2.3.3. Oxygen Radical Absorbance Capacity (ORAC)

AAPH ((2,2'-Azobis(2-methyl-propionamidine) dihydrochloride) free radical and Trolox standard were purchased from Sigma-Aldrich Hungary. Fluorescein was purchased from Fluka Analytical, Tokyo, Japan. ORAC assay was carried out in a 96-well microplate based on the method from previous study [51]. Briefly, 20 µL of the samples (1 µM final concentration, dissolved in phosphate buffer, pH = 7.4, containing 1% MeOH) were mixed with 60 µL of AAPH (12 mM final concentration, dissolved in phosphate buffer, pH = 7.4) and 120 µL of fluorescein solution (70 nM final concentration, dissolved in phosphate buffer), then the fluorescence was measured (excitation at  $\lambda = 485$  nm, and emission at  $\lambda = 520$  nm) through 3 h with 1.5-min cycle intervals with a BMG Labtech FluoStar Optima plate-reader. All experiments were carried out in triplicate, and Trolox was used as standard. The antioxidant capacity is expressed as Trolox Equivalent (TE), as calculated using GraphPad Prism 8.0 (La Jolla, CA, USA).

### 2.3.4. Xanthine Oxidase Inhibitory Activity

The xanthine oxidase (XO) inhibitory activity of the compounds was determined using continuous spectrophotometric rate based on a modified protocol of Sigma. The samples were prepared in a 96-well plate, and the final reaction mixture consisted of 10 µL of sample (dissolved in DMSO, 30 mM stock solution, 100 µM final), 100 µL of xanthine solution (0.15 mM, pH = 7.4), 140 µL of buffer (potassium phosphate, pH = 7.5) and 50 µL of XO (0.2 units/mL). When measuring the enzyme activity, control buffer was used in place of the sample. Allopurinol was applied as a control. The reaction was initiated by the automatic addition of 50 µL of XO solution. The absorbance of XO-induced uric acid production from xanthine was measured at 290 nm for 3 min in a 96-well plate on a BMG Labtech FluoStar Optima plate reader. The inhibitory percentage values were calculated by using Graph Pad Prism 8.0 (La Jolla, CA, USA).

### 2.3.5. Peroxynitrite Scavenging Activity

Peroxynitrite was synthesised by a continuous flow system using syringe pumps as published previously [52]. Briefly, an acidic solution of hydrogen peroxide (0.6 M H<sub>2</sub>O<sub>2</sub>, 0.7 M HCl) was pumped to a junction alongside of sodium nitrite solution (0.6 M) at a flow rate of 1.5 mL/min. After passing 10 cm of tubing, it was mixed with a sodium hydroxide solution (1.5 M), also pumped at 1.5 mL/min. The resulting peroxynitrite solution was a bright yellow colour. The tubing around the reaction was submerged in ice. The concentration of the solution was determined by spectrophotometry and was adjusted to 30 mM with 0.1 M NaOH solution.

In a 96-well microplate 245 µL of pyrogallol red (100 µM final concentration, dissolved in 0.1 M glycine buffer) was mixed with 50 µL of sample (0.5 mM final concentration, dissolved in DMSO) and 5 µL ONOO<sup>-</sup> solution (500 µM final concentration, freshly prepared). After mixing and keeping it at room temperature for 30 min the absorbance was measured at 550 nm using a FluoStar Optima plate reader (software version 2.20R2, BMG Labtech, Ortenberg, Germany).

### 2.3.6. COX-1 Inhibitory Activity

COX-1 inhibitory activity was tested based on the fluorometric method as described in BioVision's COX-1 inhibitor screening kit leaflet (K548-100, BioVision, CA, USA). Sample solutions were prepared by dissolving in DMSO and subsequently buffer, to get the desired concentrations. In a 96-well white plate (655101, F-bottom, Grenier bio-one, Germany), 80 µL reaction mix (containing 76 µL assay buffer, 1 µL COX Probe, 2 µL COX cofactor, and 1 µL COX-1 enzyme) was added to 10 µL sample solution, DMSO and assay buffer to

get test wells assigned for sample screen (S), negative control (N) and blank, respectively. An aliquot of 10  $\mu\text{L}$  of arachidonic/NaOH solution was added to each well using a multi-channel pipette to initiate the reaction at the same time, and the fluorescence of each well was measured kinetically at Ex/Em 550/610 nm, at 25°C for 10 min using a FluoStar Optima plate reader (BMG Labtech, Ortenberg, Germany). The COX inhibitory activity of SC560, a standard inhibitor, was also determined.

The change in fluorescence between two points, T1 and T2 were determined, and relative inhibition was calculated according to the following equation:

$$\% \text{ Inhibition} = (\Delta N - \Delta S) / \Delta N \times 100 \quad (1)$$

where N is the absorbance of the negative control, and S is that of the sample.

Dose-effect studies on the compounds were used to determine the concentration that inhibits 50% of the enzyme activity. The sigmoidal dose-response curves were obtained by using the software GraphPad Prism 8.0 (La Jolla, CA, USA), and these were used to determine the  $\text{IC}_{50}$  values of the compounds.

### 2.3.7. Physicochemical Character and Blood-brain Barrier Specific Permeability

Basic physicochemical parameters for drug design and candidate selection were calculated by Percepta Software Package (ACD/Labs, Toronto, Ontario, Canada) [53]. Tautomers and their distributions for compounds **11**, **12** and **13** were generated by Marvin Sketch and Tautomer Generator (Chemaxon Ltd., Budapest, Hungary) [54], which is freely accessible with academic license.

For kinetic aqueous solubility studies each sample was dissolved in DMSO to make 10 mM stock solutions. In a 96-well polypropylene plate (Greiner Bio-One, Kremsmünster, Austria), 15  $\mu\text{L}$  stock solutions were added to 285  $\mu\text{L}$  PBS (pH 7.4) to make starting donor solution with 500  $\mu\text{M}$  as target concentration. For each sample, 3 replicates were measured. The samples were covered and shaken at 37 °C, 300 rpm for 2 h (Heidolph Titramax 1000, Heidolph Instruments GmbH & Co. KG, Schwabach, Germany). After that, each sample was transferred into a filter plate (MSSBLPC, Multiscreen Filter plate, Merck kGaA) and filtered (Vaccum Manifold, Merck kGaA, Darmstadt, Germany). The filtrates were transferred into HPLC vials, and acetonitrile (AcN) was added to aliquot to avoid precipitation. The final solvent ratio was AcN:PBS (70:30). Filtrate concentration was determined by HPLC-UV (see Section 2.1) using 3-points calibration.

Blood-brain barrier-specific (BBB) permeability measurements were carried out using the PAMPA-BBB model. First, solutions with 500  $\mu\text{M}$  target concentration were prepared as described for the kinetic solubility study. The solutions were sonicated for 10 min at room temperature. To prepare the artificial BBB-specific membrane, 16 mg BPLe were dissolved in 600  $\mu\text{L}$  of *n*-dodecane:*n*-hexane (25:75). Each well of the donor plate (Multiscreen™-IP, MAIPNTR10, pore size 0.45  $\mu\text{m}$ , Merck kGaA) was coated with 5  $\mu\text{L}$  lipid solution and fitted into the acceptor plate containing 300  $\mu\text{L}$  PBS (pH 7.4) with 5% DMSO, and 150–150  $\mu\text{L}$  of the PBS solutions (made from the DMSO stock solutions) were placed on the donor plate's artificial membrane. The sandwich plate system was covered with a tissue of wet paper and a plastic lid to avoid evaporation of the solvent, and it was incubated at 37 °C for 4 h. In the end, the initial 500  $\mu\text{M}$  solutions ( $c_D(0)$ ), the donor ( $c_D(t)$ ) and acceptor solution ( $c_A(t)$ ) were analysed by HPLC-UV (see Section 2.1). BBB permeability was calculated using the effective permeability equation used for iso-pH conditions described by Avdeef [55] as follows.

$$P_e = \frac{-2.303}{A \cdot (t - \tau_{ss})} \cdot \left( \frac{1}{1 + r_v} \right) \cdot \lg \left[ -r_v + \left( \frac{1 + r_v}{1 - MR} \right) \cdot \frac{c_D(t)}{c_D(0)} \right] \quad (2)$$

$$MR = 1 - \frac{c_D(t)}{c_D(0)} - \frac{V_A c_A(t)}{V_D c_D(0)} \quad (3)$$

where  $A$  is the filter area ( $0.3 \text{ cm}^2$ ),  $V_D$  and  $V_A$  are the volumes in the donor ( $0.15 \text{ cm}^3$ ) and acceptor phase ( $0.3 \text{ cm}^3$ ),  $t$  is the incubation time (s),  $\tau_{ss}$  is the time to reach steady state (s),  $c_D(t)$  is the concentration of the compound in the donor phase at time point  $t$  ( $\text{mol}/\text{cm}^3$ ),  $c_D(0)$  is the concentration of the compound in the donor phase at time point zero ( $\text{mol}/\text{cm}^3$ ),  $c_A(t)$  is the concentration of the compound in the acceptor phase at time point  $t$  ( $\text{mol}/\text{cm}^3$ ),  $r_v$  is the aqueous compartment volume ratio ( $V_D/V_A$ ).

### 2.3.8. Molecular Docking

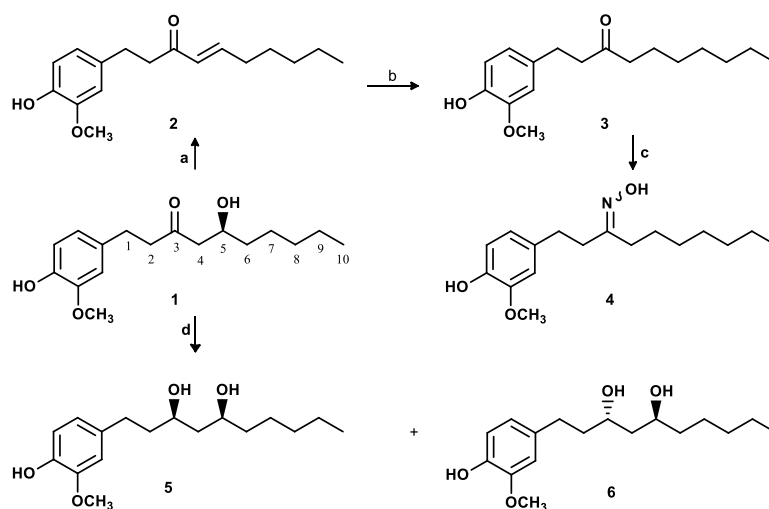
Compounds' structures were drawn and saved in PDB format using ChemDraw 12.0.2 software (ACD/LABS, Advanced Chemistry Development, Inc.). The *h*-COX-1 enzyme structure was retrieved from the PDB database. PDB files for the enzyme and compounds were converted to the PDBQT format using the graphical user interface of AutoDock4 (The Scripps Research Institute) [56]. A grid box (X:  $-33.050$ , Y:  $-47.920$ , and Z:  $0.234$ ; the number of grid points in the three dimensions [npts]: X: 40, Y: 60, and Z: 60; spacing:  $0.375$ ) was set to include the amino acids mentioned by Tóth et al. to characterize the binding site [57]. Docking parameters were set to the default values and ligands were docked via the Lamarckian algorithm. The binding energies were obtained from the resulting DLG files, and interactions visualisation was achieved via Biovia (Discovery Studio visualizer version 21.1.0.20298; Dassault Systèmes, Vélizy-Villacoublay, France) after conversion of the docked PDBQT files into PDB files using OpenBabel GUI software version 2.4.1 [58].

## 3. Results and Discussion

### 3.1. Chemistry

In this work, a commercially available ginger extract was utilised to obtain significant amounts of our selected starting material, 6-gingerol (**1**), which could be obtained in a single-step purification using flash chromatography. Using compound **1** as a starting material, 6-shogaol (**2**) was synthesised according to a literature method [43], and subsequent hydrogenation resulted in 6-paradolol (**3**) [43] in an excellent yield. The reaction of **3** with hydroxylamine hydrochloride resulted in an oxime derivative as a mixture of (*E/Z*) isomers (**4**).

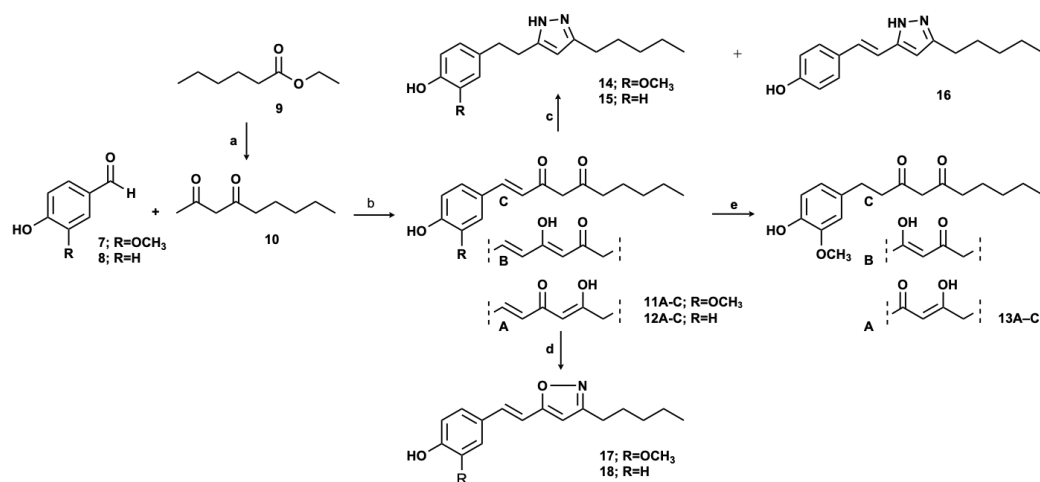
Reduction of the keto function of 6-gingerol resulted in 6-gingerdiol epimers **5** and **6** in a ratio of 3 to 2, respectively. The compounds were separated by preparative HPLC, and their structures were confirmed by HRMS and one- and two-dimensional NMR techniques, and by comparing their relevant spectral data to literature values [59–61]. Heating and cooling did not affect the stereoselectivity of the reaction. Compounds prepared directly from 6-gingerol are presented in Scheme 1.



**Scheme 1.** Semi-synthesis of compounds **2–6** from 6-gingerol (**1**). Reaction conditions: **a**. *p*TsOH/toluene/ $110 \text{ }^\circ\text{C}$ ; **b**.  $\text{H}_2/\text{Pd}/\text{C}/\text{EtOAc}/\text{r.t.}$ ; **c**.  $\text{NH}_2\text{OH}\cdot\text{HCl}/\text{EtOH}/\text{rt}$ ; **d**.  $\text{NaBH}_4/\text{MeOH}$ .



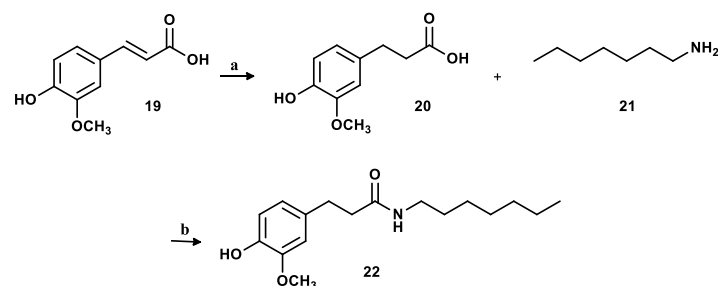
We also aimed to expand our study towards the chemical space around 6-dehydrogingerdione. To achieve this, a total synthetic approach was adopted (Scheme 2). First, 6-dehydrogingerdione (**11**) and its analogue lacking the aromatic methoxy function were synthesised starting from vanillin (**7**) or 4-hydroxybenzaldehyde (**8**) and 9-nonanedione according to a published method [44]. Catalytic hydrogenation of the double bond yielded compound **13** (6-gingerdione) [44]. The structure of compound **12** was confirmed using HRMS and NMR, and although the proton resonance of the enol methylene was not observed, the presence of carbon atoms at  $\delta_C$  201.6 and 179.6 clearly showed that **12** undergoes keto-enol tautomerisation in solution.



**Scheme 2.** Preparation of gingerdione derivatives **11–13** and their heterocyclic analogues **14–18**. Reaction conditions: a. 1. NaH/Et<sub>2</sub>O/Acetone/0 °C, 2. EtOH/HCl; b. B<sub>2</sub>O<sub>3</sub>/*i*BuNH<sub>2</sub>/DMF/90 °C; c. H<sub>6</sub>N<sub>2</sub>O/HCl/EtOH/80 °C; d. NH<sub>2</sub>OH.HCl/pyridine/ethanol/80 °C; e. H<sub>2</sub>/Pd/C/EtOAc/rt. Major tautomers of compounds **11–13** are indicated with A, B, and C.

To facilitate exploring structure–activity relationships, oxygen and nitrogen-containing heterocyclic analogues were also prepared. Interestingly, the reaction of dehydrogingerdione (**11**) and (**12**) with hydrazine monohydrate yielded two detectable products in both cases. Regarding the derivatives of **12**, both products (**15** and **16**) were successfully isolated. On the other hand, in the case of compound **11**, only compound **14** was isolated in a reasonable amount. Reactions of **11** and **12** with hydroxylamine hydrochloride resulted in oxazines **17** and **18**, respectively. Unfortunately, some of the non-protonated aromatic carbons were not detected in the <sup>13</sup>C NMR spectrum due to their long relaxation time after the irradiation, but the characteristic <sup>1</sup>H proton resonances, HRMS spectra and spectral behaviour of the compounds allowed the establishment of their chemical structures.

To investigate bioactivity changes upon replacing the keto group of compound **3** with an amide, we also prepared a capsaicin-like derivative (**22**). This was synthesised via a two-step procedure, starting with the catalytic hydrogenation of ferulic acid (**19**) to compound **20**, followed by its DCC/DMAP-mediated coupling with heptylamine (Scheme 3).



**Scheme 3.** Preparation of the amide analogue of 6-paradol (**22**). Reaction conditions: a. H<sub>2</sub>/Pd/C/EtOAc/rt; b. DCC/DMAP/CH<sub>2</sub>Cl<sub>2</sub>/rt.

### 3.2. Predicted and Experimental Physicochemical and BBB Penetration-Related Characterisation

The characterisation of the 6-gingerol derivatives was started with the determination of their physicochemical and blood–brain barrier (BBB)-specific permeability properties, which are commonly used in early-stage drug discovery. The study was carried out on two levels: (a) an in silico approach, using lead optimisation parameters and the Central Nervous System Multiparameter Optimisation (CNS MPO) compliance introduced by Wager et al. [62]; and (b) experimentally, through determination of kinetic solubility and in vitro BBB permeability of the test compounds. Predicted and experimental data are shown in Table 1.

Combining Lipinski's rule of five (Ro5) [63] and CNS MPO [62] criteria systems, the proton dissociation and lipophilicity properties of 6-gingerol derivatives were compared in a first approach. Regarding their acid–base character, the compounds can be classified into three groups: (i) monoprotic phenols (**1–6**, **17**, **18** and **22**), (ii) diprotic amphoteric (imidazole derivatives; **14–16**), and (iii) diprotic acids (gingerdione derivatives; **11–13**). The proton-dissociation behaviour of gingerdione derivatives is particularly interesting due to their tautomeric states shown in Scheme 2. The distribution % of the A-C tautomeric states of derivatives **11–13** was generated using Chemaxon Ltd.'s freely available Tautomer Generator plugin. This suggests compounds **11–13** to be mostly present in their enol forms (**A:B**, ~30:60%), while the dione forms with C-H acid function are much less expressed (**C**, ~10%). It is also important to note that, while in the case of the other gingerols (**1–6**, **14–22**) the strongest  $pK_{a,acid}$  values refer to the aromatic OH function, the  $pK_{a,acid}$  parameters indicate the proton-dissociation behaviour of the enol and dione C-H acid functions for **11–13**. Thus, based on these  $pK_{a,acid}$  values, two conclusions can be made. First, in the case of **11–13**, the stronger acid function can be assigned to the enol and C-H acid moiety, and second, the acidic character of the **A**, **B** tautomeric forms is stronger than that of the **C** forms. In terms of lipophilicity, all 6-gingerol derivatives meet the drug-likeness criterion of Ro5 ( $\log P < 5$ ). At the same time, based on the two-level risk classification created by the lead-like [64] and CNS MPO criteria ( $\log D_{pH7.4}$ ), **2–4** and **14–18** exceed (see Table 1, magenta: high violation), and **22** approach (yellow: moderate violation) the  $\log D_{pH7.4}$  violation limit. The lipophilicity values of the tautomers of **11–13** also show a marked difference. For all three compounds, the enol forms **A/B** (**11A**, **12A**, **13B**) are more lipophilic than the dione forms (**C**), which also manifests in the corresponding CNS MPO values. Regarding the next medchem parameter, the polar surface area (TPSA), all the tested gingerols satisfy both the Veber's rule ( $30\text{\AA}^2 < \text{TPSA} < 140\text{\AA}^2$ ) for bioavailability [65] and the CNS MPO range ( $40\text{\AA}^2 < \text{TPSA} < 90\text{\AA}^2$ ) [62]. CNS MPO values (physchem-based CNS compliance) of gingerols were evaluated by a three-level classification system (green–yellow–magenta) for easier overview. Compounds **1–3**, **5–6**, **11–13**, **17** and **22** (green–yellow) can be considered as suitable candidates for further CNS-targeted preclinical studies. In the case of **11–13**, due to the lipophilicity and HBD differences of the tautomers, the **C** tautomeric forms carry the optimal CNS MPO character. In addition to the predicted parameters, experimental kinetic solubility (PBS, pH 7.4) and in vitro BBB-specific permeability (PAMPA-BBB) of the compounds were also determined. Also applying a three-level classification for the kinetic solubility values, the compounds **1**, **2**, **5**, **6**, **13–15** and **22** were in the acceptable range (greater than 100  $\mu\text{M}$ ). In parallel, due to limitations resulting from poor solubility, we could only determine the permeability of these gingerols using PAMPA-BBB study. In Table 1, compounds **1**, **2**, **5**, **6** and **22** are highlighted in green ( $P_{e, BBB} \geq 25 \cdot 10^{-7}$  cm/s), for which we identified increased BBB permeability. In addition to these compounds, **14–15** are also adequate for BBB penetration. In the case of **13**, the increased hydrophilic character may impair the BBB permeability.

**Table 1.** In silico and experimental data for physicochemical and BBB permeability characterisation. Results are given as mean  $\pm$  standard error of the mean (SEM);  $n = 3$ .

Cmpds ID	Tautomer Distribution (%) <sup>b</sup>	Predicted Values <sup>a</sup>				Experimental Data		
		$pK_{a,base}/pK_{a,acid}$ <sup>c</sup>	$\log P/\log D_{pH7.4}$	TPSA	HBD/HBA	CNS MPO <sup>d</sup> [62]	Kinetic Solubility <sup>e</sup> ( $\mu\text{M}$ )	PAMPA-BBB <sup>e'</sup> $P_e$ ( $\cdot 10^{-7}$ cm/s)/MR (%)
1		-/10.0	2.9/2.9	66.8	2/4	5.06	>500	35.2 $\pm$ 2.4/23.8 $\pm$ 1.5
2		-/10.0	4.2/4.2	46.5	1/3	4.18	110.2 $\pm$ 3.8	31.7 $\pm$ 3.6/20.9 $\pm$ 3.9
3		-/10.0	4.1/4.1	46.5	1/3	4.19	45.2 $\pm$ 2.7	-/11.0 $\pm$ 0.7
4		-/10.1	4.8/4.8	62.1	2/4	3.60	75.1 $\pm$ 7.3	-/4.0 $\pm$ 11.1
5		-/10.1	3.0/3.0	69.9	3/4	4.72	>500	33.9 $\pm$ 2.5/9.1 $\pm$ 7.6
6		-/10.1	3.0/3.0	69.9	3/4	4.72	460.7 $\pm$ 10.3	27.4 $\pm$ 1.6/18.5 $\pm$ 2.7
11A	31	-/8.3	3.5/3.5	66.8	2/4	4.81		
11B	60	-/8.3	3.2/3.2	66.8	2/4	4.53		-/-
11C	9	-/8.7	3.3/3.3	63.6	1/4	5.01		
12A	38	-/8.3	3.9/3.8	57.5	2/3	4.62		
12B	54	-/8.4	3.4/3.4	57.5	2/3	4.15		-/-
12C	8	-/8.9	3.5/3.5	54.4	1/3	4.75		
13A	31	-/8.7	3.4/3.4	66.8	2/4	4.58		
13B	60	-/8.7	3.5/3.4	66.8	2/4	4.56		-/-
13C	9	-/9.4	3.3/3.3	63.6	1/4	4.98		
14		3.8/10.1	4.7/4.7	58.1	2/4	3.67	276.7 $\pm$ 5.5	15.8 $\pm$ 0.8/33.6 $\pm$ 4.6
15		3.9/10.1	4.9/4.9	48.9	2/3	3.57	202.9 $\pm$ 5.5	20.7 $\pm$ 4.3/3.1 $\pm$ 5.7
16		3.1/10.0	4.8/4.8	48.9	2/3	3.59	89.4 $\pm$ 3.1	-/-
17		-/9.9	4.4/4.4	55.5	1/4	4.04	10.9 $\pm$ 2.0	-/-
18		-/9.8	4.8/4.8	46.3	1/3	3.87	<LOD	-/-
22		-/10.1	3.6/3.6	58.6	2/4	4.36	482.6 $\pm$ 18.7	32.2 $\pm$ 3.4/12.1 $\pm$ 5.2
Aspirin		-/3.5	1.4/-1.7	63.6	1/4	5.75	-	-

<sup>a</sup> Predicted values calculated by ACD/Labs Percepta software [53], <sup>b</sup> Generated by Chemaxon Tautomer Generator [54], <sup>c</sup> strongest acidic  $pK_a$ , <sup>d</sup> CNS MPO were determined using predicted  $pK_{a,basic}$ ,  $\log P/\log D_{pH7.4}$  (classic and consensus settings, respectively), TPSA and HBD values, <sup>e/e'</sup> after 2 h/4 h, at 37 °C in PBS, pH 7.4. Colours of classification systems:  $\log D_{pH7.4}$ : moderate violation (yellow)  $\geq 3.5$ , high violation (magenta)  $\geq 4.0$ ; CNS MPO: low (magenta)  $\leq 4.0$ , moderate (yellow)  $\leq 4.7$ , good (green)  $> 4.7$ ; Kin.Sol.: low (magenta)  $\leq 100$ , moderate (yellow)  $\leq 300$ , good (green)  $> 300$ ; Increased BBB-permeability (green)  $> 25$ .

### 3.3. Antiplatelet Aggregation and COX-1 Inhibition Activity of the Compounds

The arachidonic acid (AA)-cyclooxygenase-1 (COX-1) pathway plays an important role in platelet activation [66]. Aspirin, the standard antiplatelet drug, can prevent AA metabolism to thromboxane A2 by inhibiting COX-1, and thus exert antiplatelet effects [67]. To evaluate similar bioactivities of 6-gingerol (**1**) and its derivatives, the compounds were tested for their inhibitory effects on AA-induced platelet aggregation. Compounds **3**, **2**, **17**, **16**, and **13** showed the most promising results, with IC<sub>50</sub> values of around 2–4 μM, respectively, while the effects of 6-gingerol (**1**) and aspirin were up to 22 and 50 times weaker, respectively (Table 2).

**Table 2.** Antiplatelet and Cyclooxygenase-1 (COX-1) inhibition assay results. For antiplatelet activity, washed human platelets were treated with gingerol derivatives for 3 min and then stimulated with arachidonic acid (100 μM); data are presented as mean ± SEM, *n* = 3 for antiplatelet and *n* = 2 for COX-1 inhibition assay; aspirin was used as a positive control.

Compound	Antiplatelet IC <sub>50</sub> (μM)	LLE <sup>a</sup> <sub>(Antiplatelet)</sub>	COX-1 IC <sub>50</sub> (μM)	LLE <sup>a</sup> <sub>(COX-1)</sub>
<b>1</b>	45.9 ± 5.1	1.46	62.5 ± 23.8	1.30
<b>2</b>	2.8 ± 0.5	1.40	9.8 ± 0.6	0.81
<b>3</b>	2.1 ± 1.0	1.56	4.4 ± 0.2	1.26
<b>4</b>	5.2 ± 0.4	0.47	5.2 ± 0.3	0.48
<b>5</b>	51.7 ± 2.7	1.26	54.3 ± 6.5	1.27
<b>6</b>	45.1 ± 6.0	1.32	76.2 ± 0.3	1.12
<b>11(A)</b> <sup>b</sup>	4.1 ± 1.0	1.89 <sup>b</sup>	23.1 ± 9.3	1.14
<b>12(A)</b> <sup>b</sup>	71.7 ± 28.3	0.24 <sup>b</sup>	>200	-
<b>13(B)</b> <sup>b</sup>	3.6 ± 0.9	1.94 <sup>b</sup>	11.8 ± 5.4	1.53
<b>14</b>	4.1 ± 1.2	0.72	3.6 ± 0.2	0.74
<b>15</b>	>100	-	>200	-
<b>16</b>	3.5 ± 0.9	0.63	17.5 ± 0.1	-0.04
<b>17</b>	3.1 ± 0.9	1.08	5.85 ± 0.04	0.83
<b>18</b>	32.0 ± 10.1	-0.27	>200	-
<b>22</b>	35.9 ± 23.7	0.80	>100	-
<b>Aspirin</b>	106.0 ± 20.2	2.58	-	-

<sup>a</sup> Ligand–lipophilic efficiency: LLE = pIC<sub>50</sub> – logP<sub>predicted</sub>. For LLE, green colouring indicates a satisfactory level (LLE<sub>(Antiplatelet)</sub> ≥ 1.5 or LLE<sub>(COX-1)</sub> ≥ 1.0 and IC<sub>50</sub> ≤ 10 μM). <sup>b</sup> For the sake of strict characterisation, the tautomer with the highest logP value (see Table 1) was included in the LLE calculation for compounds **11**–**13**, i.e., the value for the worst possible case is shown in the table.

The antiplatelet mechanism of action of 6-gingerol and its derivatives has previously been suggested to be COX-1 inhibition [37,68,69]. The results obtained for the newly synthesised compounds are in accordance with this notion. The IC<sub>50</sub> datasets of Table 2 give a linear correlation coefficient (R<sup>2</sup>) value of 0.887 (Supplementary Materials, Figure S26), strongly suggesting that COX-1 inhibition is indeed the mechanism behind the observed antiplatelet action.

Concerning structure–activity relationships, our results suggest the importance of an aromatic methoxy group, as seen by comparing the IC<sub>50</sub> values of **11** vs. **12**, **14** vs. **15**, and **17** vs. **18**. Interestingly, this rule did not apply for compound **16**. This may underline a possible role of the Δ<sup>1,2</sup> olefin in some cases, e.g., when it is conjugated with a pyrazole ring. Presence of the 5-OH group is highly unfavourable; its elimination (as in compounds **2**, **3**, and **4**) increased antiplatelet activity by ca. an order of magnitude, as well as its oxidation (compound **13** vs. **1**) or replacement by a heterocycle (e.g., compound **14** vs. **1**).

Compound **22**, in which the β-keto alcohol function of compound **1** was replaced by an amide group, showed only moderate activity. Notably, however, replacing the 3-oxo group by an oxime group led to only a slight, ca. 2-fold decrease in the antiplatelet activity (IC<sub>50</sub> = 5.2 μM), while this chemical change opened the way to diverse further functionalisation possibilities.

Our results come in accordance with previous reports on compound **3**, i.e., 6-paradol that is naturally present in ginger roots.

Since the mid-2000s, the entropic or lipophilicity-driven lead optimisation constraint has mainly been observed in CNS-targeted drug discovery, significantly increasing the number of clinical candidates that were promiscuous or otherwise carrying off-target effects and toxicity risks [70]. To reduce this issue, several ligand efficiency metrics have been introduced [71], which can be used to filter out this effect. In this context, in our study, the  $IC_{50}$  data obtained on the two biological targets were evaluated using the ligand-lipophilic efficiency (LLE =  $pIC_{50} - \log P$ ) metric [70]. After, a two-conditions-based lead selection was performed using the  $IC_{50}$  and LLE values, where the LLE values of 6-gingerol derivatives with an  $IC_{50} \leq 10 \mu M$  and an LLE value higher than 1.0 were highlighted (Table 2, compounds coloured green for LLE<sub>Antipatelet</sub>: **2**, **3**, **11**, **13** and **17** and LLE<sub>COX-1</sub>: **3**). Summarizing the data in Tables 1 and 2, due to the strict selection, only compound **2** can be assigned as a primary candidate for further preclinical studies, while compounds **3**, **11** and **17** are potential leads that require an appropriate formulation to improve their aqueous solubility. From the point of view of lead optimisation, compound **3** is particularly interesting, satisfying the LLE/ $IC_{50}$  screening criteria for both biological targets. Compound **13** can also be identified as a secondary lead, for which the further goal may be fine-tuning the BBB permeability property.

#### 3.4. Molecular Docking

Compounds were docked using AutoDock4 into the human COX-1 enzyme crystal structure retrieved from the Protein Data Bank (PDB ID: 6Y3C). Grid parameters were set to centre at residue Ser530 and to include residues Tyr385, Arg120, and Tyr348 that are in the COX-1 binding pocket [57]. In the cases of compounds **11**, **12**, and **13**, the tautomeric forms A–C were subjected to in silico docking. Detailed results of the docking study are provided as Supplementary Materials, Table S1.

The highest binding affinity ( $-9.5$  Kcal/mol) was found for the new isoxazole-containing compound **17**, which was also among the most potent antiplatelet derivatives. Tóth et al. discussed the importance of Tyr385 and Ser530 in the irreversible binding of aspirin to COX-1 active site [46]; notably, the docking results showed hydrogen bonding interactions with Ser530 in the case of compound **1**, **4**, and **6**, while compounds **11B**, **12A**, and **22** appeared to interact via hydrogen bonds with Tyr385 (Table S1). Interestingly, compound **17** did not show any of the above-mentioned interaction with either of these amino acids (Figure 1).

#### 3.5. Antioxidant Assay

Antioxidant activity was assessed using multiple models, including DDPH, ORAC, ONOO<sup>-</sup> scavenging, and XO inhibition assays; results are shown in Table 3. Compounds **5**, **17**, **4**, **1**, and **11** showed the best activity in the diphenyl-2-picrylhydrazyl (DPPH) scavenging capacity assay. Among these, compound **5** is clearly the most promising antioxidant lead, considering its DPPH-scavenging  $IC_{50}$  value, its ORAC value, which is more than twice as much as that of Trolox, and its predicted and experimental pharmacokinetic parameters. Interestingly, compound **6**, the 3-epimer variant of **5**, showed only ca. half of the activity of **5** in the DPPH assay and was also weaker in terms of ORAC. Similar to the results obtained for the antiplatelet and COX-1 inhibition assay, the importance of an aromatic methoxy group for potent DPPH scavenging activity was highlighted; except for compound **16**, all compounds without this moiety (**12**, **15**, and **18**) were inactive in this regard. Concerning their ORAC values, however, compounds **12** and **16** were the most potent among all compounds, which highlights the complementary value of these two bioassays to evaluate free radical scavenging activity of small molecule antioxidants.

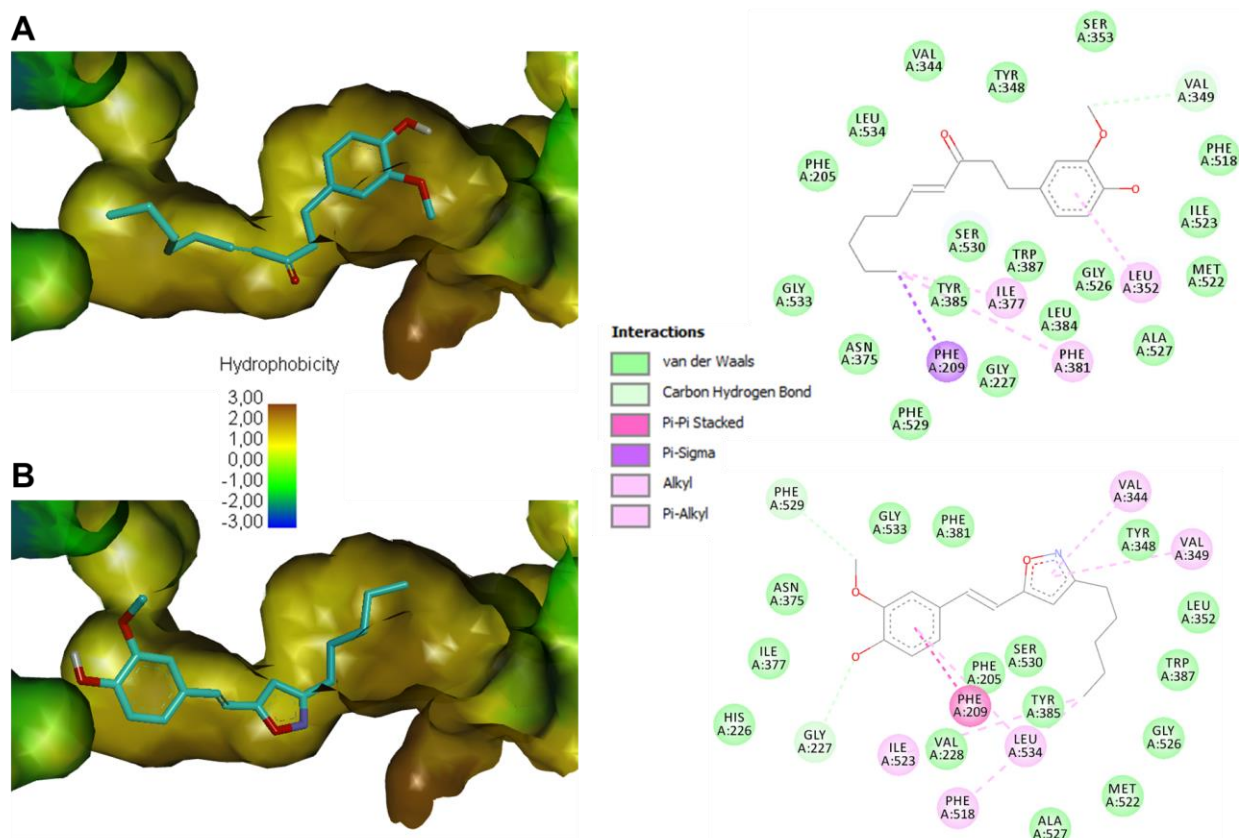


**Figure 1.** The binding mode of compounds **2** (A) and **17** (B) on *h*-COX-1 enzyme (PDB ID: 6Y3C) visualised with Discovery studio visualizer (21.1.0.20298); 3D orientation with the enzyme's hydrophobicity surface to the left and 2D representation of the observed interactions to the right. Colour codes for A and B are identical.

**Table 3.** The antioxidant activity results of 6-gingerol and its derivatives. Values are given as mean  $\pm$  standard error of the mean (SEM). ORAC assay results are given in Trolox equivalents (TE), ONOO<sup>-</sup> scavenging and xanthine oxidase (XO) inhibition assay results are given in % inhibition at concentrations of 500 and 100  $\mu$ M, respectively;  $n = 2$  for DPPH;  $n = 3$  for ORAC, ONOO<sup>-</sup> and XO.

	DDPH		ORAC TE	ONOO <sup>-</sup> Scavenging (%)	XO Inhibition (%)
	IC <sub>50</sub> ( $\mu$ M)	LLE <sup>a</sup>			
<b>1</b>	8.92 $\pm$ 0.46	2.15	1.30 $\pm$ 0.04	<5.0	<5.0
<b>2</b>	11.41 $\pm$ 0.49	0.75	1.10 $\pm$ 0.03	<5.0	<5.0
<b>3</b>	9.43 $\pm$ 0.16	0.93	1.36 $\pm$ 0.02	<5.0	<5.0
<b>4</b>	8.56 $\pm$ 0.07	0.27	0.47 $\pm$ 0.09	<5.0	10.56 $\pm$ 2.30
<b>5</b>	6.51 $\pm$ 0.28	2.19	2.30 $\pm$ 0.05	<5.0	<5.0
<b>6</b>	13.82 $\pm$ 0.03	1.86	1.12 $\pm$ 0.03	<5.0	<5.0
<b>11</b>	9.04 $\pm$ 0.19	1.54	1.98 $\pm$ 0.12	<5.0	<5.0
<b>12</b>	>200	-	2.89 $\pm$ 0.49	<5.0	<5.0
<b>13</b>	10.86 $\pm$ 0.69	1.46	2.60 $\pm$ 0.06	<5.0	<5.0
<b>14</b>	16.16 $\pm$ 0.46	0.09	0.44 $\pm$ 0.07	<5.0	10.13 $\pm$ 1.65
<b>15</b>	>200	-	1.00 $\pm$ 0.02	<5.0	12.30 $\pm$ 0.90
<b>16</b>	18.98 $\pm$ 1.63	-0.08	2.88 $\pm$ 0.16	<5.0	16.01 $\pm$ 4.05
<b>17</b>	8.13 $\pm$ 0.21	0.69	0.77 $\pm$ 0.20	38.40 $\pm$ 3.05	<5.0
<b>18</b>	>100	-	1.76 $\pm$ 0.06	5.64 $\pm$ 1.31	<5.0
<b>22</b>	14.07 $\pm$ 0.21	1.25	1.62 $\pm$ 0.004	<5.0	<5.0
<b>allopurinol</b>	-	-	-	-	98.80 $\pm$ 0.11

<sup>a</sup> Ligand-lipophilic efficiency: LLE =  $pIC_{50} - \log P_{\text{predicted}}$ . For LLE, green colouring indicates a satisfactory level (LLE  $\geq$  1.5 and IC<sub>50</sub>  $\leq$  10  $\mu$ M).

#### 4. Conclusions

In this study, a combined semi- and total synthetic strategy was adopted to prepare fourteen 6-gingerol derivatives including eight new compounds, which were subsequently characterised as antiplatelet and COX-1 inhibitor agents, and free radical scavenger or XO inhibitor antioxidants. The compounds' pharmacodynamic and pharmacokinetic characterisation revealed 6-shogaol (**2**) to be the best lead as a cardiovascular protective agent, and compounds **3**, **11**, and **17** as new starting points for hit-to-lead optimisation. The 3,5-diol compound **5** was identified as a more potent and less promiscuous antioxidant than its parent compound 6-gingerol (**1**) or its 3-epimer compound **6**. Due to its favourable pharmacokinetic parameters, compound **5** is also suggested as a potential CNS-specific antioxidant. Further studies to evaluate this notion are to be conducted soon.

**Supplementary Materials:** The following Supplementary Materials can be downloaded at: <https://www.mdpi.com/article/10.3390/antiox12030744/s1>, Figures S1–S8: HRMS spectra for compounds **4**, **12**, **14–18** and **22**, Figures S9–S24: <sup>1</sup>H and <sup>13</sup>C NMR spectra for compounds **4**, **12**, **14–18** and **22**, Figure S25: Correlation between the antiplatelet and COX-1 inhibitory activities of the tested compounds; Table S1: Docking results obtained using AutoDockTools 1.5.7 and Discovery Studio visualizer (21.1.0.20298).

**Author Contributions:** Conceptualisation, T.G. and A.H.; methodology, S.H.H.A. and T.G.; software, G.T.B.; investigation, S.H.H.A., T.G., O.G.A., G.G., R.B., N.K., M.-C.T. and G.T.B.; resources, G.T.B. and A.H.; data curation, S.H.H.A., and G.T.B.; writing—original draft preparation, S.H.H.A., T.G., G.T.B. and A.H.; writing—review and editing, T.G., G.T.B. and A.H.; supervision, C.-C.W., G.T.B. and A.H.; funding acquisition, A.H. All authors have read and agreed to the published version of the manuscript.

**Funding:** This research has been funded by the National Research, Development and Innovation Office, Hungary (NKFIH; K-134704), and TKP2021-EGA-32 by the Ministry of Innovation and Technology, Hungary.

**Institutional Review Board Statement:** Not applicable.

**Informed Consent Statement:** Not applicable.

**Data Availability Statement:** The data presented in this study are available in the article and Supplementary Materials.

**Acknowledgments:** The authors would like to acknowledge Magdi A. M. Elhussein for his insights regarding the molecular docking section.

**Conflicts of Interest:** The authors declare no conflict of interest.

#### References

1. Yahyazadeh, R.; Rahimi, V.B.; Yahyazadeh, A.; Mohajeri, S.A.; Askari, V.R. Promising effects of gingerol against toxins: A review article. *Biofactors* **2021**, *47*, 885–913. [[CrossRef](#)]
2. Fakhri, S.; Patra, J.K.; Das, S.K.; Das, G.; Majnooni, M.B.; Farzaei, M.H. Ginger and Heart Health: From Mechanisms to Therapeutics. *Curr. Mol. Pharmacol.* **2020**, *14*, 943–959. [[CrossRef](#)] [[PubMed](#)]
3. Roudsari, N.M.; Lashgari, N.; Momtaz, S.; Roufogalis, B.; Abdolghaffari, A.H.; Sahebkar, A. Ginger: A complementary approach for management of cardiovascular diseases. *Biofactors* **2021**, *47*, 933–951. [[CrossRef](#)]
4. Mao, Q.-Q.; Xu, X.-Y.; Cao, S.-Y.; Gan, R.-Y.; Corke, H.; Beta, T.; Li, H.-B. Bioactive Compounds and Bioactivities of Ginger (*Zingiber officinale* Roscoe). *Foods* **2019**, *8*, 185. [[CrossRef](#)]
5. Saxena, R.; Rida, P.C.G.; Kucuk, O.; Aneja, R. Ginger augmented chemotherapy: A novel multitarget nontoxic approach for cancer management. *Mol. Nutr. Food Res.* **2016**, *60*, 1364–1373. [[CrossRef](#)] [[PubMed](#)]
6. Sp, N.; Kang, D.; Lee, J.-M.; Bae, S.; Jang, K.-J. Potential Antitumor Effects of 6-Gingerol in p53-Dependent Mitochondrial Apoptosis and Inhibition of Tumor Sphere Formation in Breast Cancer Cells. *Int. J. Mol. Sci.* **2021**, *22*, 4660. [[CrossRef](#)]
7. Alharbi, K.S.; Nadeem, M.S.; Afzal, O.; Alzarea, S.I.; Altamimi, A.S.A.; Almalki, W.H.; Mubeen, B.; Iftikhar, S.; Shah, L.; Kazmi, I. Gingerol, a Natural Antioxidant, Attenuates Hyperglycemia and Downstream Complications. *Metabolites* **2022**, *12*, 1274. [[CrossRef](#)]

8. Almatroodi, S.; Alnuqaydan, A.; Babiker, A.; Almogbel, M.; Khan, A.; Rahmani, A.H. 6-Gingerol, a Bioactive Compound of Ginger Attenuates Renal Damage in Streptozotocin-Induced Diabetic Rats by Regulating the Oxidative Stress and Inflammation. *Pharmaceutics* **2021**, *13*, 317. [CrossRef]
9. Hughes, T.; Azim, S.; Ahmad, Z. Inhibition of Escherichia coli ATP synthase by dietary ginger phenolics. *Int. J. Biol. Macromol.* **2021**, *182*, 2130–2143. [CrossRef] [PubMed]
10. Hayati, R.F.; Better, C.D.; Denis, D.; Komarudin, A.G.; Bowolaksono, A.; Yohan, B.; Sasmono, R.T. [6]-Gingerol Inhibits Chikungunya Virus Infection by Suppressing Viral Replication. *BioMed Res. Int.* **2021**, *2021*, 6623400. [CrossRef]
11. Abolaji, A.O.; Ojo, M.; Afolabi, T.T.; Arowoogun, M.D.; Nwawolor, D.; Farombi, E.O. Protective properties of 6-gingerol-rich fraction from Zingiber officinale (Ginger) on chlorpyrifos-induced oxidative damage and inflammation in the brain, ovary and uterus of rats. *Chem. Biol. Interact.* **2017**, *270*, 15–23. [CrossRef]
12. Adetuyi, B.O.; Farombi, E.O. 6-Gingerol, an active constituent of ginger, attenuates lipopolysaccharide-induced oxidation, inflammation, cognitive deficits, neuroplasticity, and amyloidogenesis in rat. *J. Food Biochem.* **2021**, *45*, e13660. [CrossRef]
13. Liao, Y.-R.; Leu, Y.-L.; Chan, Y.-Y.; Kuo, P.-C.; Wu, T.-S. Anti-Platelet Aggregation and Vasorelaxing Effects of the Constituents of the Rhizomes of Zingiber officinale. *Molecules* **2012**, *17*, 8928–8937. [CrossRef] [PubMed]
14. Liu, L.; Yao, L.; Wang, S.; Chen, Z.; Han, T.; Ma, P.; Jiang, L.; Yuan, C.; Li, J.; Ke, D.; et al. 6-Gingerol Improves Ectopic Lipid Accumulation, Mitochondrial Dysfunction, and Insulin Resistance in Skeletal Muscle of Ageing Rats: Dual Stimulation of the AMPK/PGC-1 $\alpha$  Signaling Pathway via Plasma Adiponectin and Muscular AdipoR1. *Mol. Nutr. Food Res.* **2019**, *63*, e1800649. [CrossRef] [PubMed]
15. Guo, X.; Zhang, Y.; Wang, T.; Wang, X.; Xu, Y.; Wang, Y.; Qiu, J. Ginger and 6-gingerol prevent lipopolysaccharide-induced intestinal barrier damage and liver injury in mice. *J. Sci. Food Agric.* **2021**, *102*, 1066–1075. [CrossRef] [PubMed]
16. Poltronieri, J.; Becceneri, A.B.; Fuzer, A.M.; Filho, J.C.C.; Martin, A.C.B.M.; Vieira, P.C.; Pouliot, N.; Cominetti, M.R. [6]-gingerol as a Cancer Chemopreventive Agent: A Review of Its Activity on Different Steps of the Metastatic Process. *Mini Rev. Med. Chem.* **2014**, *14*, 313–321. [CrossRef]
17. Ahmed, S.H.H.; Gonda, T.; Hunyadi, A. Medicinal chemistry inspired by ginger: Exploring the chemical space around 6-gingerol. *RSC Adv.* **2021**, *11*, 26687–26699. [CrossRef]
18. WHO. Cardiovascular Diseases. Available online: [https://www.who.int/health-topics/cardiovascular-diseases#tab=tab\\_1](https://www.who.int/health-topics/cardiovascular-diseases#tab=tab_1) (accessed on 9 March 2023).
19. Koupenova, M.; Kehrel, B.E.; Corkrey, H.A.; Freedman, J.E. Thrombosis and platelets: An update. *Eur. Heart J.* **2017**, *38*, 785–791. [CrossRef]
20. Passacquale, G.; Sharma, P.; Perera, D.; Ferro, A. Antiplatelet therapy in cardiovascular disease: Current status and future directions. *Br. J. Clin. Pharmacol.* **2022**, *88*, 2686–2699. [CrossRef]
21. Ornelas, A.; Zacharias-Millward, N.; Menter, D.G.; Davis, J.S.; Lichtenberger, L.; Hawke, D.; Hawk, E.; Vilar, E.; Bhattacharya, P.; Millward, S. Beyond COX-1: The effects of aspirin on platelet biology and potential mechanisms of chemoprevention. *Cancer Metastasis Rev.* **2017**, *36*, 289–303. [CrossRef]
22. Khodadi, E. Platelet Function in Cardiovascular Disease: Activation of Molecules and Activation by Molecules. *Cardiovasc. Toxicol.* **2020**, *20*, 1–10. [CrossRef]
23. Farhady, S.; Kobarfard, F.; Saghaie, L.; Rostami, M. Synthesis and Antiplatelet Activity Evaluation of a Group of Novel Ethyl Acetoacetate Phenylhydrazone Derivatives. *Iran. J. Pharm. Res.* **2021**, *20*, 307–315. [CrossRef] [PubMed]
24. Pirozzi, E.J.; Wills, B.K. Antiplatelet Drug Toxicity. In *StatPearls*; StatPearls Publishing LLC.: Treasure Island, FL, USA, 2021.
25. Cortellini, G.; Caruso, C.; Romano, A. Aspirin challenge and desensitization: How, when and why. *Curr. Opin. Allergy Clin. Immunol.* **2017**, *17*, 247–254. [CrossRef]
26. Shim, Y.K.; Kim, N. Nonsteroidal Anti-inflammatory Drug and Aspirin-Induced Peptic Ulcer Disease. *Korean J. Gastroenterol.* **2016**, *67*, 300–312. [CrossRef]
27. McEwen, B.J. The Influence of Herbal Medicine on Platelet Function and Coagulation: A Narrative Review. *Semin. Thromb. Hemost.* **2015**, *41*, 300–314. [CrossRef] [PubMed]
28. McEwen, B.J. The Influence of Diet and Nutrients on Platelet Function. *Semin. Thromb. Hemost.* **2014**, *40*, 214–226. [CrossRef] [PubMed]
29. Abebe, W. Herbal medication: Potential for adverse interactions with analgesic drugs. *J. Clin. Pharm. Ther.* **2002**, *27*, 391–401. [CrossRef]
30. Mousa, S.A. Antithrombotic Effects of Naturally Derived Products on Coagulation and Platelet Function. *Breast Cancer* **2010**, *663*, 229–240. [CrossRef]
31. Chen, C.; Zhang, Q.; Wang, F.-Q.; Li, C.-H.; Hu, Y.-J.; Xia, Z.-N.; Yang, F.-Q. In vitro anti-platelet aggregation effects of fourteen fruits and vegetables. *Pak. J. Pharm. Sci.* **2019**, *32*, 185–195.
32. Young, H.-Y.; Liao, J.-C.; Chang, Y.-S.; Luo, Y.-L.; Lu, M.-C.; Peng, W.-H. Synergistic Effect of Ginger and Nifedipine on Human Platelet Aggregation: A Study in Hypertensive Patients and Normal Volunteers. *Am. J. Chin. Med.* **2006**, *34*, 545–551. [CrossRef]
33. Bordia, A.; Verma, S.K.; Srivastava, K.C. Effect of ginger (Zingiber officinale Rosc.) and fenugreek (Trigonella foenumgraecum L.) on blood lipids, blood sugar and platelet aggregation in patients with coronary artery disease. *Prostaglandins Leukot. Essent. Fat. Acids* **1997**, *56*, 379–384. [CrossRef]



34. Jiang, X.; Williams, K.M.; Liauw, W.S.; Ammit, A.J.; Roufogalis, B.D.; Duke, C.C.; Day, R.O.; McLachlan, A.J. Effect of ginkgo and ginger on the pharmacokinetics and pharmacodynamics of warfarin in healthy subjects. *Br. J. Clin. Pharmacol.* **2005**, *59*, 425–432. [[CrossRef](#)] [[PubMed](#)]
35. Lumb, A.B. Effect of Dried Ginger on Human Platelet Function. *Thromb. Haemost.* **1994**, *71*, 110–111. [[CrossRef](#)]
36. Shih, H.-C.; Chern, C.-Y.; Kuo, P.-C.; Wu, Y.-C.; Chan, Y.-Y.; Liao, Y.-R.; Teng, C.-M.; Wu, T.-S. Synthesis of Analogues of Gingerol and Shogaol, the Active Pungent Principles from the Rhizomes of *Zingiber officinale* and Evaluation of Their Anti-Platelet Aggregation Effects. *Int. J. Mol. Sci.* **2014**, *15*, 3926–3951. [[CrossRef](#)]
37. Koo, K.L.; Ammit, A.J.; Tran, V.H.; Duke, C.C.; Roufogalis, B. Gingerols and Related Analogues Inhibit Arachidonic Acid-Induced Human Platelet Serotonin Release and Aggregation. *Thromb. Res.* **2001**, *103*, 387–397. [[CrossRef](#)]
38. Dugasani, S.; Pichika, M.R.; Nadarajah, V.D.; Balijepalli, M.K.; Tandra, S.; Korlakunta, J.N. Comparative antioxidant and anti-inflammatory effects of [6]-gingerol, [8]-gingerol, [10]-gingerol and [6]-shogaol. *J. Ethnopharmacol.* **2010**, *127*, 515–520. [[CrossRef](#)] [[PubMed](#)]
39. Han, X.; Liu, P.; Zheng, B.; Zhang, M.; Zhang, Y.; Xue, Y.; Liu, C.; Chu, X.; Wang, X.; Sun, S.; et al. 6-Gingerol exerts a protective effect against hypoxic injury through the p38/Nrf2/HO-1 and p38/NF- $\kappa$ B pathway in H9c2 cells. *J. Nutr. Biochem.* **2022**, *104*, 108975. [[CrossRef](#)] [[PubMed](#)]
40. Ho, S.-C.; Chang, Y.-H. Comparison of Inhibitory Capacities of 6-, 8- and 10-Gingerols/Shogaols on the Canonical NLRP3 Inflammasome-Mediated IL-1 $\beta$  Secretion. *Molecules* **2018**, *23*, 466. [[CrossRef](#)]
41. Tong, Y.; Wang, Z.; Cai, L.; Lin, L.; Liu, J.; Cheng, J. NLRP3 Inflammasome and Its Central Role in the Cardiovascular Diseases. *Oxidative Med. Cell. Longev.* **2020**, *2020*, 4293206. [[CrossRef](#)] [[PubMed](#)]
42. Toldo, S.; Mezzaroma, E.; Buckley, L.F.; Potere, N.; Di Nisio, M.; Biondi-Zoccai, G.; Van Tassell, B.W.; Abbate, A. Targeting the NLRP3 inflammasome in cardiovascular diseases. *Pharmacol. Ther.* **2022**, *236*, 108053. [[CrossRef](#)] [[PubMed](#)]
43. Wei, C.-K.; Tsai, Y.-H.; Korinek, M.; Hung, P.-H.; El-Shazly, M.; Cheng, Y.-B.; Wu, Y.-C.; Hsieh, T.-J.; Chang, F.-R. 6-Paradol and 6-Shogaol, the Pungent Compounds of Ginger, Promote Glucose Utilization in Adipocytes and Myotubes, and 6-Paradol Reduces Blood Glucose in High-Fat Diet-Fed Mice. *Int. J. Mol. Sci.* **2017**, *18*, 168. [[CrossRef](#)]
44. Yao, J.; Ge, C.; Duan, D.; Zhang, B.; Cui, X.; Peng, S.; Liu, Y.; Fang, J. Activation of the Phase II Enzymes for Neuroprotection by Ginger Active Constituent 6-Dehydrogingerdione in PC12 Cells. *J. Agric. Food Chem.* **2014**, *62*, 5507–5518. [[CrossRef](#)]
45. Kumboonma, P.; Senawong, T.; Saenglee, S.; Yenjai, C.; Phaosiri, C. Identification of phenolic compounds from *Zingiber officinale* and their derivatives as histone deacetylase inhibitors and antioxidants. *Med. Chem. Res.* **2017**, *26*, 650–661. [[CrossRef](#)]
46. Murphree, S.S.; Mason, J.D.; Bean, T.G.; Perry, M.C. Rapid Aqueous Borohydride Reduction of Carbonyls Under Sealed-Tube Microwave Conditions. *Synth. Commun.* **2012**, *42*, 1979–1986. [[CrossRef](#)]
47. Balaji, N.V.; Ramani, M.V.; Viana, A.G.; Sanglard, L.P.; White, J.; Mulabagal, V.; Lee, C.; Gana, T.J.; Egiebor, N.O.; Subbaraju, G.V.; et al. Design, synthesis and in vitro cell-based evaluation of the anti-cancer activities of hispolon analogs. *Bioorg. Med. Chem.* **2015**, *23*, 2148–2158. [[CrossRef](#)] [[PubMed](#)]
48. Szakonyi, Z.; Gonda, T.; Ötvös, S.B.; Fülöp, F. Stereoselective syntheses and transformations of chiral 1,3-aminoalcohols and 1,3-diols derived from nopinone. *Tetrahedron Asymmetry* **2014**, *25*, 1138–1145. [[CrossRef](#)]
49. Lin, Y.T.; Li, Y.; Hsu, H.C.; Tsai, J.Y.; Lee, J.H.; Tai, C.J.; Wu, M.J.; Wu, C.C. Discovery of 7, 4'-dimethoxy-3-hydroxyflavone as a protease-activated receptor 4 antagonist with antithrombotic activity and less bleeding tendency in mice. *Biochem. Pharmacol.* **2022**, *202*, 115152. [[CrossRef](#)]
50. Fukumoto, L.R.; Mazza, G. Assessing Antioxidant and Prooxidant Activities of Phenolic Compounds. *J. Agric. Food Chem.* **2000**, *48*, 3597–3604. [[CrossRef](#)] [[PubMed](#)]
51. Mielnik, M.B.; Rzeszutek, A.; Triumf, E.C.; Egelandsdal, B. Antioxidant and other quality properties of reindeer muscle from two different Norwegian regions. *Meat Sci.* **2011**, *89*, 526–532. [[CrossRef](#)] [[PubMed](#)]
52. Fási, L.; Latif, A.D.; Zupkó, I.; Lévai, S.; Dékány, M.; Béni, Z.; Könczöl, Á.; Balogh, G.T.; Hunyadi, A. AAPH or Peroxynitrite-Induced Biorelevant Oxidation of Methyl Caffate Yields a Potent Antitumor Metabolite. *Biomolecules* **2020**, *10*, 1537. [[CrossRef](#)]
53. *Percepta*; v2021.2.1 Build 3525; ACD/Labs: Toronto, ON, Canada, 2021.
54. *Marvin Sketch, Tautomer Generator*; 20.21.0; Chemaxon: Budapest, Hungary, 2020.
55. Avdeef, A. Permeability Equations. In *Absorption and Drug Development: Solubility, Permeability, and Charge State*; Avdeef, A., Ed.; Wiley Interscience: Hoboken, NJ, USA, 2012; pp. 465–481.
56. Morris, G.M.; Huey, R.; Lindstrom, W.; Sanner, M.F.; Belew, R.K.; Goodsell, D.S.; Olson, A.J. AutoDock4 and AutoDockTools4: Automated docking with selective receptor flexibility. *J. Comput. Chem.* **2009**, *30*, 2785–2791. [[CrossRef](#)] [[PubMed](#)]
57. Tóth, L.; Muszbek, L.; Komáromi, I. Mechanism of the irreversible inhibition of human cyclooxygenase-1 by aspirin as predicted by QM/MM calculations. *J. Mol. Graph. Model.* **2013**, *40*, 99–109. [[CrossRef](#)] [[PubMed](#)]
58. O'Boyle, N.M.; Banck, M.; James, C.A.; Morley, C.; Vandermeersch, T.; Hutchison, G.R. Open Babel: An open chemical toolbox. *J. Cheminform.* **2011**, *3*, 33. [[CrossRef](#)]
59. Rychnovsky, S.D.; Skalitzky, D.J. Stereochemistry of alternating polyol chains:  $^{13}\text{C}$  NMR analysis of 1,3-diol acetonides. *Tetrahedron Lett.* **1990**, *31*, 945–948. [[CrossRef](#)]
60. Lv, L.; Chen, H.; Soroka, M.; Chen, X.; Leung, T.; Sang, S. 6-Gingerdiols as the Major Metabolites of 6-Gingerol in Cancer Cells and in Mice and Their Cytotoxic Effects on Human Cancer Cells. *J. Agric. Food Chem.* **2012**, *60*, 11372–11377. [[CrossRef](#)]

61. Kikuzaki, H.; Tsai, S.-M.; Nakatani, N. Gingerdiol related compounds from the rhizomes of *Zingiber officinale*. *Phytochemistry* **1992**, *31*, 1783–1786. [[CrossRef](#)]
62. Wager, T.T.; Hou, X.; Verhoest, P.R.; Villalobos, A. Central Nervous System Multiparameter Optimization Desirability: Application in Drug Discovery. *ACS Chem. Neurosci.* **2016**, *7*, 767–775. [[CrossRef](#)] [[PubMed](#)]
63. Lipinski, C.A.; Lombardo, F.; Dominy, B.W.; Feeney, P.J. Experimental and computational approaches to estimate solubility and permeability in drug discovery and development settings. *Adv. Drug Deliv. Rev.* **2001**, *23*, 3–25. [[CrossRef](#)]
64. Tinworth, C.P.; Young, R.J. Facts, Patterns, and Principles in Drug Discovery: Appraising the Rule of 5 with Measured Physico-chemical Data. *J. Med. Chem.* **2020**, *63*, 10091–10108. [[CrossRef](#)]
65. Veber, D.F.; Johnson, S.R.; Cheng, H.-Y.; Smith, B.R.; Ward, K.W.; Kopple, K.D. Molecular Properties That Influence the Oral Bioavailability of Drug Candidates. *J. Med. Chem.* **2002**, *45*, 2615–2623. [[CrossRef](#)]
66. Badimon, L.; Vilahur, G.; Rocca, B.; Patrono, C. The key contribution of platelet and vascular arachidonic acid metabolism to the pathophysiology of atherothrombosis. *Cardiovasc. Res.* **2021**, *117*, 2001–2015. [[CrossRef](#)] [[PubMed](#)]
67. Crescente, M.; Menke, L.; Chan, M.V.; Armstrong, P.C.; Warner, T.D. Eicosanoids in platelets and the effect of their modulation by aspirin in the cardiovascular system (and beyond). *Br. J. Pharmacol.* **2019**, *176*, 988–999. [[CrossRef](#)] [[PubMed](#)]
68. Nurtjahja-Tjendraputra, E.; Ammit, A.; Roufogalis, B.; Tran, V.H.; Duke, C.C. Effective anti-platelet and COX-1 enzyme inhibitors from pungent constituents of ginger. *Thromb. Res.* **2003**, *111*, 259–265. [[CrossRef](#)] [[PubMed](#)]
69. Guh, J.-H.; Ko, F.-N.; Jong, T.-T.; Teng, C.-M. Antiplatelet Effect of Gingerol Isolated from *Zingiber officinale*. *J. Pharm. Pharmacol.* **1995**, *47*, 329–332. [[CrossRef](#)]
70. Leeson, P.D.; Springthorpe, B. The influence of drug-like concepts on decision-making in medicinal chemistry. *Nat. Rev. Drug Discov.* **2007**, *6*, 881–890. [[CrossRef](#)]
71. Tarcsay, Á.; Keserű, G.M. Contributions of Molecular Properties to Drug Promiscuity. *J. Med. Chem.* **2013**, *56*, 1789–1795. [[CrossRef](#)]

**Disclaimer/Publisher’s Note:** The statements, opinions and data contained in all publications are solely those of the individual author(s) and contributor(s) and not of MDPI and/or the editor(s). MDPI and/or the editor(s) disclaim responsibility for any injury to people or property resulting from any ideas, methods, instructions or products referred to in the content.